1-1-2021

Smart pansharpening approach using kernel-based image filtering

Ahmad A.L. Smadi
Xidian University

Shuyuan Yang
Xidian University

Atif Mehmood
Xidian University

Ahed Abugabah
Zayed University, ahed.abugabah@zu.ac.ae

Min Wang
Xidian University

See next page for additional authors

Recommended Citation

Author First name, Last name, Institution

Ahmad A.L. Smadi, Shuyuan Yang, Atif Mehmood, Ahed Abugabah, Min Wang, and Muzaffar Bashir

ORIGINAL RESEARCH PAPER

Smart pansharpening approach using kernel-based image filtering

Ahmad AL Smadi[1] [ID] | **Shuyuan Yang**[1] | **Atif Mehmood**[1] | **Ahed Abugabah**[2] | **Min Wang**[3] | **Muzaffar Bashir**[4]

[1] School of Artificial Intelligence, Xidian University, No. 2 South Taibai Road, Xian, China

[2] College of Technological Innovation, Zayed University, Abu Dhabi, UAE

[3] Key Laboratory of Radar Signal Processing, Xidian University, Xi'an, China

[4] Department of Physics, University of the Punjab, Lahore, Pakistan

Correspondence
Shuyuan Yang, School of Artificial Intelligence, Xidian University, No. 2 South Taibai Road, Xian 710071, China.
Email: syyang@xidian.edu.cn

Abstract

Remote sensing image fusion plays important roles in numerous applications, including monitoring, metrology, and agriculture. Image fusion gathers essential information from several image sources and consolidates them into a single image called a fused image. The fused image involves relevant data, and it is more informative than any other images extracted from one source. This study proposed a pansharpening technique based on image filtering utilising a bilateral filter to generate high-frequency details from panchromatic image. The various types of side window guided filters are employed to enhance the multispectral band from panchromatic image and then used these filters to adjust spatial data misfortune that happens when images are combined. Experimental results demonstrated that the proposed method provides consistent results concise with reported by the previous research in terms of subjective and objective assessments on remote sensing data.

1 | INTRODUCTION

Image fusion is the way toward integrating two or more images into one image. It helps detectable human quality since it joins correlative information of images. Pansharpening consolidates high-spatial panchromatic (PAN) and multispectral (MS) images to create high-resolution multispectral images (HRMS). Remote sensing satellite images are broadly utilised in numerous applications, such as monitoring, metrology, agriculture, planning applications, and military [1, 2], and so forth. Most of the satellite sensors provide high spatial resolution PAN and several MS bands, which lead to difficulty for having a high-resolution multispectral image (HRMS). Along these lines, numerous techniques for the fusion of (MS) and (PAN) images have been proposed. To date, deep learning-based methods provide promising results in many domains, such as image processing, image fusion and computer vision [3, 4]. Recently, various pansharpening techniques have been implemented [5–7] to fuse PAN and MS images to acquire HRMS. The essential part of such strategies is the extraction of the detailed information from the PAN image,

thus, transferring the detailed information to the corresponding MS image. The component substitution (CS) [8] methods and multi-resolution-analysis (MRA) [9] methods are considered conventional methods. The conventional methods are used for extracting detailed information from PAN image. Some of the eminent CS-based strategies are IHS [10], PCA [11], GS [12], and more recently developed methods belong to this class [13, 14] in which these techniques often provide fusion results that suffers from spectral distortion [15]. In contrast, MRA based methods, for example, Laplacian pyramid [16] and transforms based on wavelets [17–19], can keep spectral information excellently. The fusion result of these methods may suffer spatial distortion. In the fields of image processing and fusion, numerous applications including the idea of image filtering to denoise, deblur, and image enhancement. In order to overcome some of these previously mentioned shortcomings and to acquire a high-resolution multispectral image, we extend the side window filtering with three kinds of filters, namely, Guided filter (GF), Gradient guided filter (GGF), and Weighted guided filter (WGF). Particularly our work is focused on the use of a
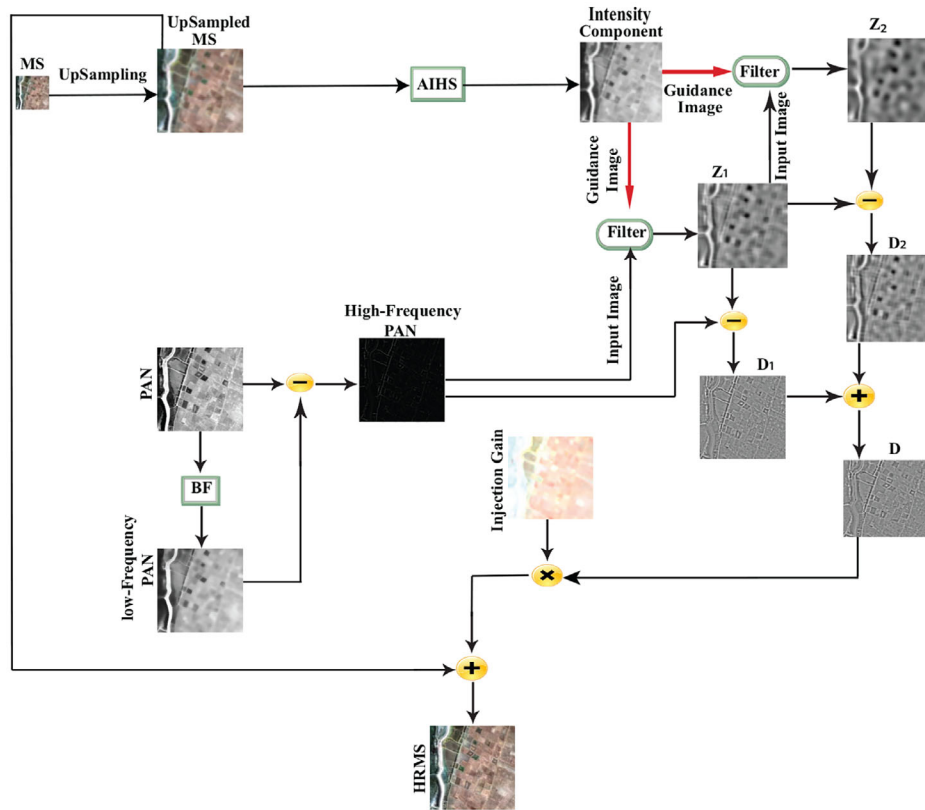
FIGURE 1 Flowchart of the proposed method, MS and PAN are the multispectral image and panchromatic image, respectively. BF is the bilateral filter. D is the detailed map. Z is the filtered image (an approximation image of the input image). HRMS is the fused result

FIGURE 2 Detailed examination of parameter setting. (a–c) the impact of ξ on fusion performance when $r = 2$, (d–f) the impact of ξ on fusion performance when $r = 4$ and (g–i) the impact of ξ on fusion performance when $r = 8$

FIGURE 3 Fusion results of QuickBird degraded dataset

side window, unlike traditional approaches which use full window regression. Therefore, the proposed techniques produced improved results in terms of pansharpening.

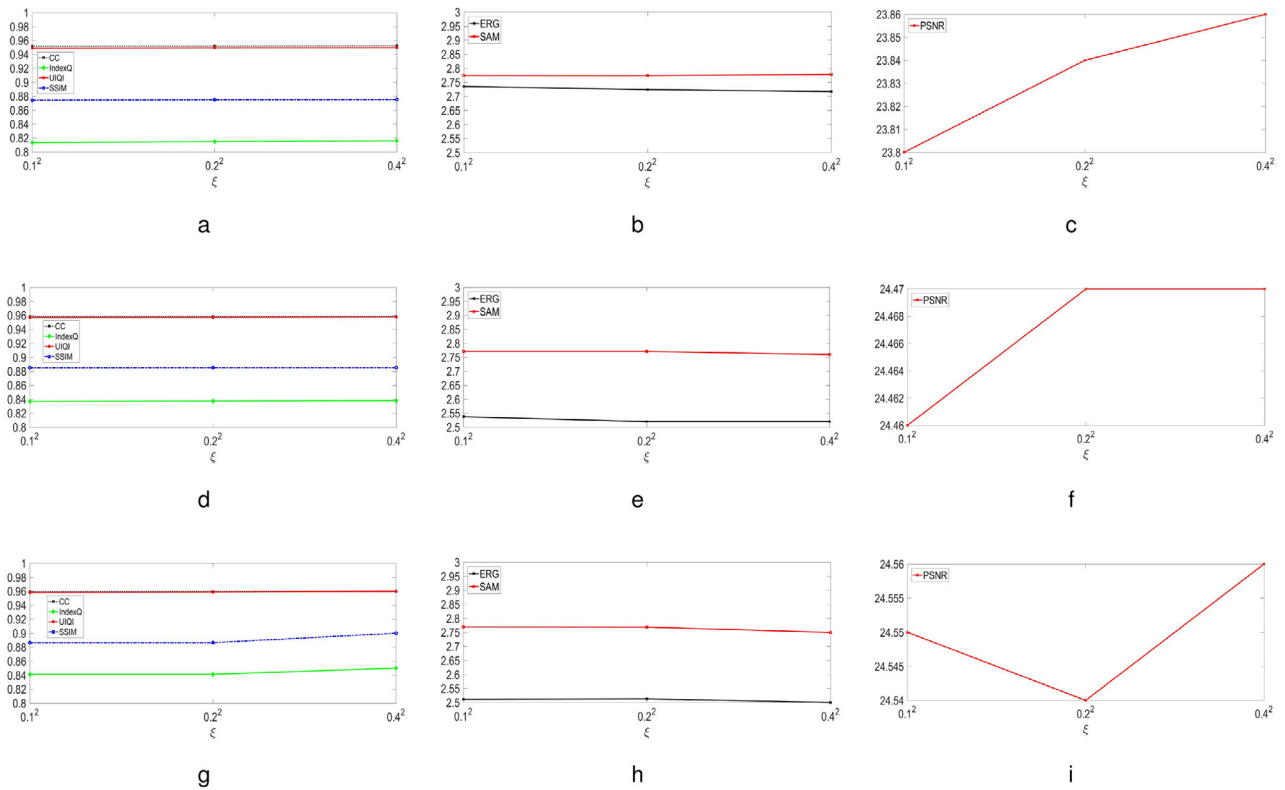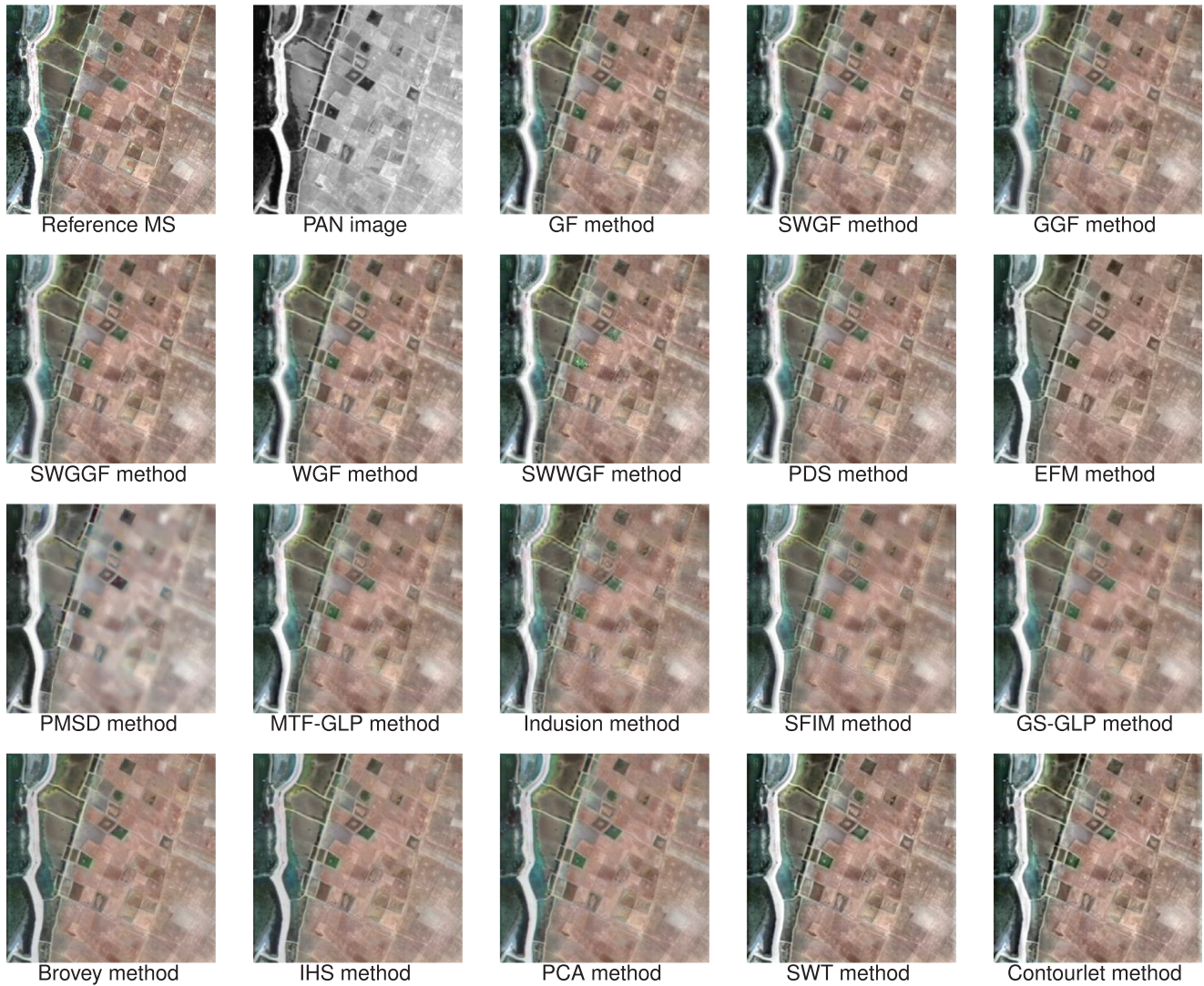At this stage, different filters have been introduced, for example, box filters, Gaussian filters, and median filters etc. These filters are utilised in image deblurring, honing edge discovery and highlight extraction. Numerous applications require image filtering, which can protect edges and provide image enhancement. In recent years, the GF was elaborated as an edge-preserving and smoothing operator. Lihua et al. [20] introduced a pansharpening method (PDS) based on dual-scale detail extraction using a GF.

Xu et al. [21] proposed a pansharpening approach based on a guided filter (EFM), which only used a PAN image for detail extraction. In [6], the authors introduced a pansharpening method using multi-scale decomposition (PMSD). Thereby, methods are focused on spatial details.

In view of the fact that the edge-preserving image filtering can be categorised into [22] (1) Global optimisation-based methods, for instance, weighted least square smoothing [23], Nonlinear total variation [24]. (2) Local optimisation-based techniques, for example, bilateral filter [25], GF [26]. Accordingly, locally-based filters consistently endeavour to evaluate a yield of a pixel that depends on its neighbours. Approximately no matter what, the pixel being handled is situated at the focal point of an activity window, and different pixels in the activity window are its neighbours. For example, side window filtering (SWF) technique, that aligns the window's side or corner with the pixel being processed [27]. Inspired by side window filtering, we extended the various types of guided-image-filtering to exploit these filters benefits and performances. In the proposed method, different types of GFs based on side windows are implemented to acquire HRMS. The main contributions of this paper can be outlined as:

TABLE 1 Numerical evaluation for QuickBird degraded dataset

Method	CC (1)	RMSE (0)	ERG (0)	SAM (0)	IndexQ (1)	UIQI (1)	SSIM↑	PSNR↑
GF	0.9361	0.2589	2.945	3.3152	0.8266	0.9344	0.8935	23.5953
SWGF	**0.9384**	**0.2458**	**2.857**	3.316	**0.8370**	**0.9358**	0.8936	**24.062**
WGF	0.9363	0.2586	2.9402	3.3153	0.8246	0.9332	0.8936	23.6049
SWWGF	0.9303	0.2703	3.0707	3.3147	0.8098	0.9288	0.8862	23.2208
GGF	0.8924	0.3337	3.7942	3.3152	0.7572	0.8784	0.861	21.3972
SWGGF	0.8948	0.3303	3.7591	3.3152	0.7697	0.8803	0.8651	21.4852
PDS	0.9320	0.2682	3.0413	3.3727	0.8067	0.928	0.8877	23.2837
EFM	0.9381	0.2495	2.8664	4.4523	0.8302	0.9356	0.8777	23.991
PMSD	0.9035	0.3608	4.2395	6.7113	0.7412	0.8983	0.7251	20.7272
MTF-GLP	0.92144	0.2554	2.9243	3.7878	0.8012	0.9348	0.8840	23.7242
Indusion	0.91806	0.2761	3.1483	3.5524	0.7395	0.9197	0.8608	23.0412
SFIM	0.9351	0.2622	2.9819	**3.3046**	0.7670	0.9298	0.8828	23.4853
Brovey	0.9299	0.2789	3.2003	3.3105	0.7801	0.9120	0.8959	22.9532
IHS	0.9298	0.2774	3.2015	3.4987	0.7864	0.9111	0.8963	23.0000
PCA	0.93743	0.2476	2.8855	3.6063	0.7998	0.9317	**0.9040**	23.8562
GS-GLP	0.9357	0.2572	2.9532	3.8289	0.7958	0.9327	0.8830	23.6586
SWT	0.9364	0.2541	2.9453	3.7847	0.8179	0.9355	0.8867	23.7551
Contourlet	0.9265	0.2731	3.1813	4.1396	0.8042	0.9260	0.8702	23.1196
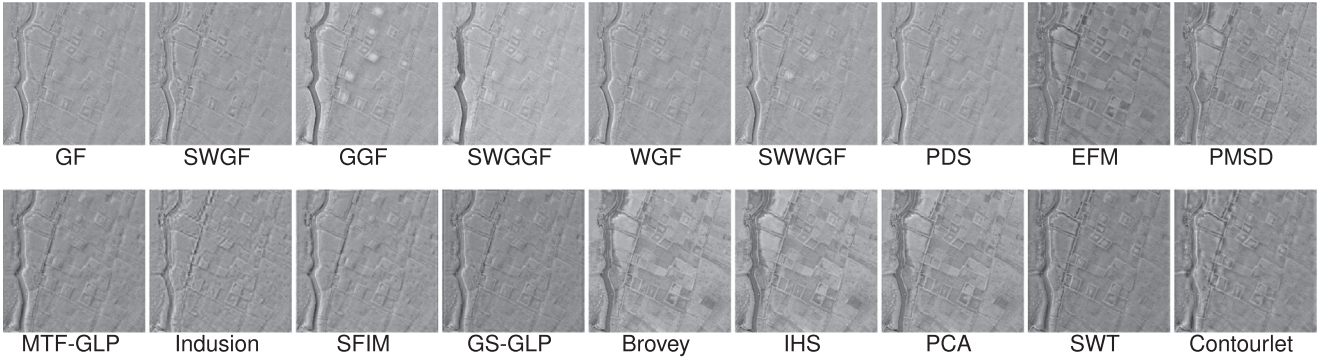
FIGURE 4 Error maps indicate the structural uniformity and edges for degraded QuickBird dataset

- The bilateral filter is utilised to generate frequency components from panchromatic image.
- Side window filtering is employed with different types of GFs. Thus, we utilised these filters to minimise the difference between the intensity components image and the low-pass filtered PAN image. And to perceive how these filters are working.

2 | RELATED WORK

2.1 | Bilateral filter

A bilateral filter (BF) is defined as a nonlinear, edge-preserving, noise decreasing and smoothing filters for images. The BF takes into consideration the varying intensities in the neighbour pixels for edge-preserving [25]. In a similar way, the BF replaces every pixel's intensity with a weighted average of intensity values calculated from neighbour pixels. The BF can divide the image into two parts; filtered image and residual image [28]. The BF depends on two parameters which are $\sigma s, \sigma r$ to measure the amount of filtering for an input image [29]. Thus, the following formulas represent the estimation of BF:

$$\text{BF} = \frac{1}{W_p} \sum_{x_i \in w} G\sigma s(\|x_i - x\|) G\sigma r\left(\|I_{x_i} - I_x\|\right) I_{x_i} \quad (1)$$

$$W_p = \sum_{x_i \in w} G\sigma s(\|x_i - x\|) G\sigma r\left(\|I_{x_i} - I_x\|\right) \quad (2)$$

where w denotes the window centred in x, x represents the coordinates of the current pixel to be filtered, x_i is a pixel that
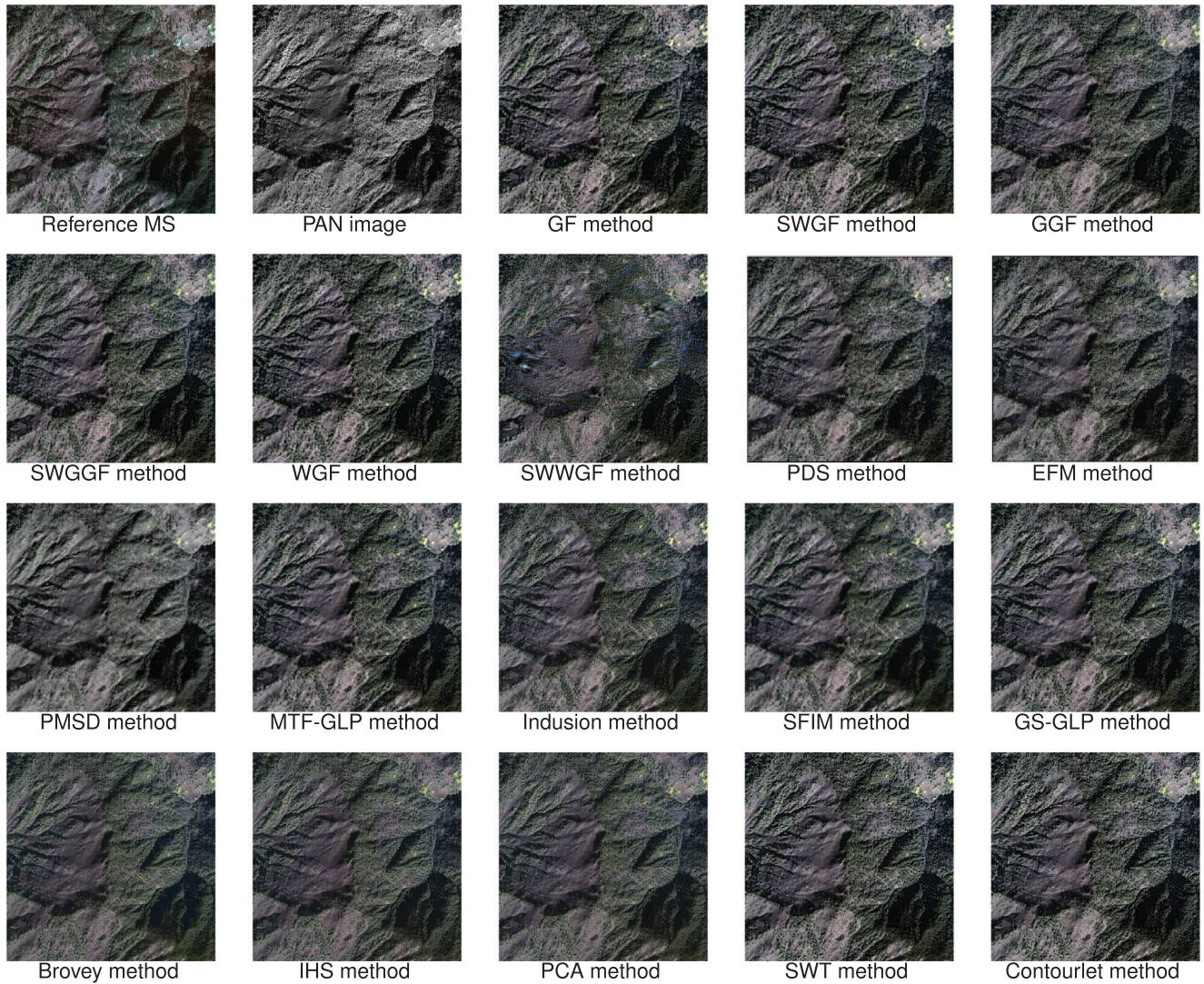
FIGURE 5 Fusion results of Ikonos degraded dataset

belongs to w, I indicates the input image to be filtered, $G\sigma s$, $G\sigma r$ are a spatial Gaussian and a range Gaussian, respectively. W_p indicates a normalisation factor.

2.2 | Guided filter

The edge-preserving filters are witnessed an increased interest by the researchers. They have been a hot topic in recent years due to the applications of these filters in several areas, including image denoising, scene improvement for additional examination. The GF has been described as one of the most popular edge-preserving filters used in many applications [30], such as image enhancement and image matting. The GF uses a guidance image to enhance the input image. However, the GF depends on two parameters, a filter radius r and a regulation ξ that is an important operator to obtain edge preserving. The

following equations illustrate the general function of guided image filtering.

$$O_i = a_i G_i + b_i, \forall i \in w_i \qquad (3)$$

$$a_i = \frac{\text{cov}(G_i, I_i)}{\text{var}(G_i) + \xi}, b_i = \bar{I}_i - a_i \bar{G} \qquad (4)$$

where w_i a square window of a filter radius $(2r+1)(2r+1)$, a_i and b_i are constant linear coefficients in the window w_i, I is the input image, and G denotes the guidance image.

In view of the GF instruction, the GF accomplishes filtering utilising a local linear transform of a guidance image. Then again, the GF has been appeared to create haloing artefacts in some cases [26], which thus prompted the improvement of increasingly versatile filters, for instance, WGF [31] and GGF [32].
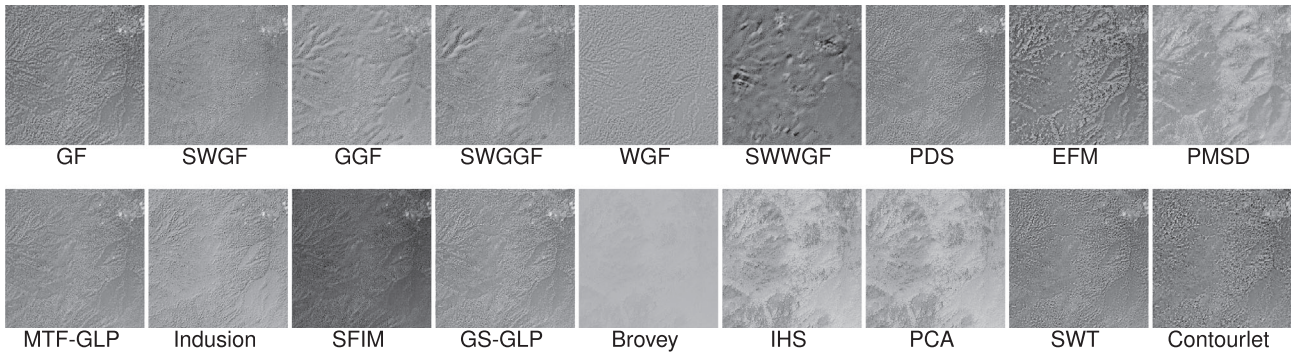
FIGURE 6   Error maps indicate the structural uniformity and edges for degraded Ikonos dataset

FIGURE 7   Fusion results of degraded GeoEye dataset

2.3 | Side window filtering

In numerous applications that utilise the type of filtering algorithm, there has been noticeably a need to smooth out real noise, save edges and other sign subtleties simultaneously. SWF centres around three kinds of ordinary edges, step edge, incline edge, and rooftop edge. SWF focuses on the pixel as a potential edge and produces several neighbourhood windows (named as

TABLE 2 Numerical evaluation for Ikonos degraded dataset

Method	CC (1)	RMSE (0)	ERG (0)	SAM (0)	IndexQ (1)	UIQI (1)	SSIM↑	PSNR↑
GF	0.9270	0.2800	6.2653	12.8257	0.8621	0.9230	0.8176	22.8934
SWGF	0.9262	0.2808	6.2818	12.3288	0.8618	0.9224	0.8199	22.8671
WGF	**0.9401**	**0.2433**	**5.4253**	11.6593	0.8698	**0.9362**	**0.8288**	**24.0620**
SWWGF	0.8148	0.4143	9.2297	11.967	0.7119	0.8087	0.7444	19.4813
GGF	0.9187	0.2800	6.2417	11.0938	0.8353	0.9138	0.8110	22.8784
SWGGF	0.9217	0.2751	6.1370	11.1013	0.8416	0.9172	0.8151	23.0348
PDS	0.9238	0.2836	6.3353	13.9839	0.8701	0.9191	0.8080	22.7649
EFM	0.8998	0.3225	7.3420	16.0964	**0.8769**	0.8917	0.7734	21.376
PMSD	0.8967	0.3351	7.4034	12.8148	0.8101	0.8872	0.7042	21.3093
MTF-GLP	0.9274	0.2554	5.7250	12.1920	0.8720	0.9318	0.8238	23.6422
Indusion	0.8927	0.3015	6.5607	12.0265	0.8286	0.9000	0.7925	22.5083
SFIM	0.9329	0.2603	5.8328	**10.6116**	0.8600	0.9305	0.8244	23.5230
Brovey	0.9012	0.3115	6.9436	10.7899	0.8206	0.8760	0.7860	21.9636
IHS	0.8740	0.3284	7.2999	11.7035	0.8183	0.8653	0.7697	21.4841
PCA	0.9014	0.3127	6.9530	11.3104	0.8229	0.8773	0.7850	21.9070
GS-GLP	0.9318	0.2623	5.9530	12.6899	0.8764	0.9283	0.8239	23.4217
SWT	0.9066	0.3177	7.3049	15.9003	0.8696	0.8972	0.7939	21.7311
Contourlet	0.8956	0.3354	7.7282	16.6019	0.8602	0.8856	0.7796	21.2538

TABLE 3 Numerical evaluation for GeoEye degraded dataset

Method	CC (1)	RMSE (0)	ERG (0)	SAM (0)	IndexQ (1)	UIQI (1)	SSIM↑	PSNR↑
GF	0.9192	0.3691	5.2684	7.2381	0.7326	0.9189	0.8615	20.4301
SWGF	0.9191	0.3698	5.2793	7.2498	0.7326	0.9187	0.8615	20.4135
WGF	**0.9313**	**0.3399**	**4.8624**	7.1320	0.7295	**0.9274**	**0.8725**	**21.1617**
SWWGF	0.7222	0.6503	9.6274	8.1282	0.5491	0.7003	0.7519	15.316
GGF	0.9161	0.3873	5.5752	**7.1182**	0.6779	0.8952	0.8456	20.0829
SWGGF	0.9222	0.3718	5.3454	7.1182	0.6911	0.9050	0.8541	20.4283
PDS	0.9223	0.3578	5.1455	7.8224	0.7299	0.9197	0.8627	20.7775
EFM	0.8557	0.4748	6.8131	12.414	0.7507	0.8424	0.7405	18.1640
PMSD	0.8651	0.4944	7.005	10.760	0.7009	0.8374	0.7272	18.0366
MTF-GLP	0.9274	0.3494	4.9895	7.9831	0.7513	0.924	0.8715	20.8655
Indusion	0.9019	0.4007	5.723	8.2434	0.6933	0.8977	0.8464	19.6895
SFIM	0.9300	0.3508	5.0149	7.2426	0.7323	0.9243	0.8679	20.8851
Brovey	0.9271	0.3915	5.6459	7.2196	0.6642	0.8974	0.8471	19.9960
IHS	0.9259	0.3996	5.7706	7.6827	0.6697	0.8784	0.8408	19.8207
PCA	0.8638	0.4810	6.9996	9.9914	0.6644	0.8245	0.7891	18.2215
GS-GLP	0.9262	0.3666	5.2490	8.4755	0.7511	0.9233	0.8704	20.5260
SWT	0.9126	0.3776	5.4212	9.2655	**0.7547**	0.9112	0.8467	20.1819
Contourlet	0.8807	0.4381	6.2853	11.1329	0.7420	0.8786	0.7957	18.8685

side windows) around it, every one of which adjusts the objective pixel to a side or a corner (rather than the focal point) of the window. The yield of SWF is a direct blend of the neighbours in one of the side windows, which can be best inexact the objective pixels. SWF technique is an effective and practical

edge-preserving filtering solution. Hui Yin et al. [27, 33] defined the SW in the continuous case, starting from the flat line then, changing θ which represents the edge between flat line and window while fixing the position of target pixel $i(x, y)$, therefore, we able to alter the course of the window while adjusting its side
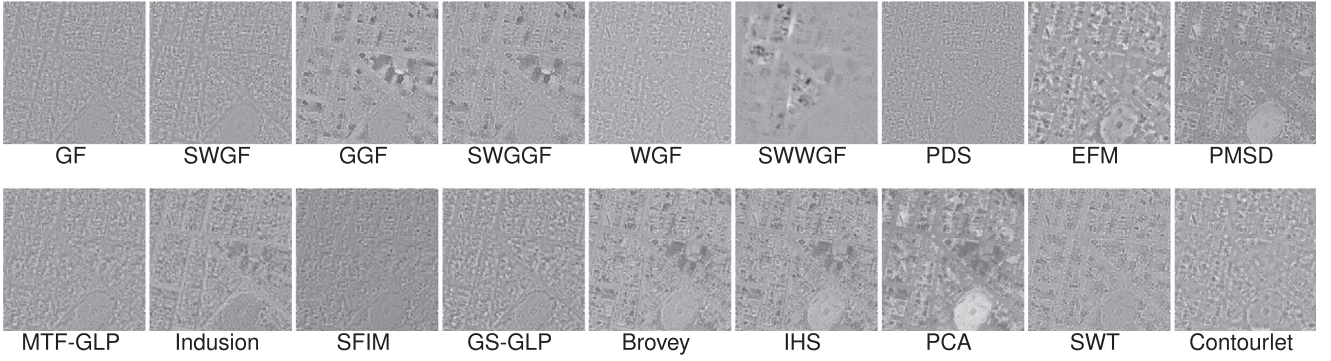
FIGURE 8 Error maps indicate the structural uniformity and edges for degraded GeoEye dataset

to i. In view of that, we had eight possible filter kernels which are, down, right, up, left, southwest, southeast, northeast, and northwest. Furthermore, the main explicit prerequisite is that the target pixel is set on the side or corner of the window. The following equations illustrate the operation of SWF.

$$I_i^{\theta,\rho,r} = F(q_i, \theta, \rho, r), \forall \theta = k \times \frac{\Pi}{2}, k \in [0, 3] \text{ and } \rho \in \{0, r\} \tag{5}$$

By minimising the distance between the input and output, especially at the edge, the minimum $L2$ distance is being chosen.

$$I'_{\text{SWF}} = \underset{\forall I'_i, \rho, r}{\arg\min} \left\| q_i - I_i^{\theta,\rho,r} \right\|_2^2 \tag{6}$$

where r indicates the radius of the window and F represents the kernel filter.

3 | MATERIALS AND METHODS

In this study, we proposed a pansharpening technique based on side window image filtering, which is an effective edge-preserving filter. The pipeline of the proposed scheme is shown in Figure 1. The proposed scheme consists of a series of steps as follows.

- Firstly, generate the high-frequency component of PAN image by utilising the bilateral filter BF.
- Secondly, utilise an adaptive intensity hue saturation (AIHS) [34] to generate the MS image's Intensity component.
- Thirdly, employ various types of side window filtering to filter the high-frequency PAN image to obtain the approximation image by using I component as a guided image.
- Fourthly, compute injection gain for each band of MS, which is defined by the quantity of the panchromatic image spatial detail information, which is being injected into the MS image.
- Finally, the high-resolution MS image is generated.

3.1 | Generating high frequency components

In order to obtain a high-frequency component of PAN image, the bilateral filter is utilised as it performs better in holding edge subtleties. Therefore, by subtracting the original image from the filtered image, the high-frequency component is acquired.

$$\text{PAN}_L = \text{BF}(\text{PAN}_L, G\sigma_s, G\sigma_r) \tag{7}$$

$$\text{PAN}_H = \text{PAN} - \text{PAN}_L \tag{8}$$

where BF denotes the bilateral filter function, PAN_L, PAN_H indicate the low-frequency components and high-frequency components of PAN image, respectively.

3.2 | Generating intensity component from MS image

The intensity hue saturation IHS strategy produces an image with a high spatial resolution while suffers from spectral distortions. The general formula for generating an intensity component is illustrated as follows:

$$I = \sum_{i=1}^{N} \alpha_i MS_{i'\text{th}} \tag{9}$$

where α_i represents the weight coefficients, and N represents the number of spectral bands. The Optimal weights can be obtained by solving the following optimisation problem [34]:

$$\alpha_i^* = \underset{\alpha_i}{\arg\min} \left\| \text{PAN} - \sum_{i=1}^{N} \alpha_i \mathbf{M} S_{i'\text{th}} \right\|^2 \tag{10}$$

3.3 | Implementing different types of guided filter

In this step, three different types of the guided filter were used. Namely, guided filter GF weighted guided filter WGF and
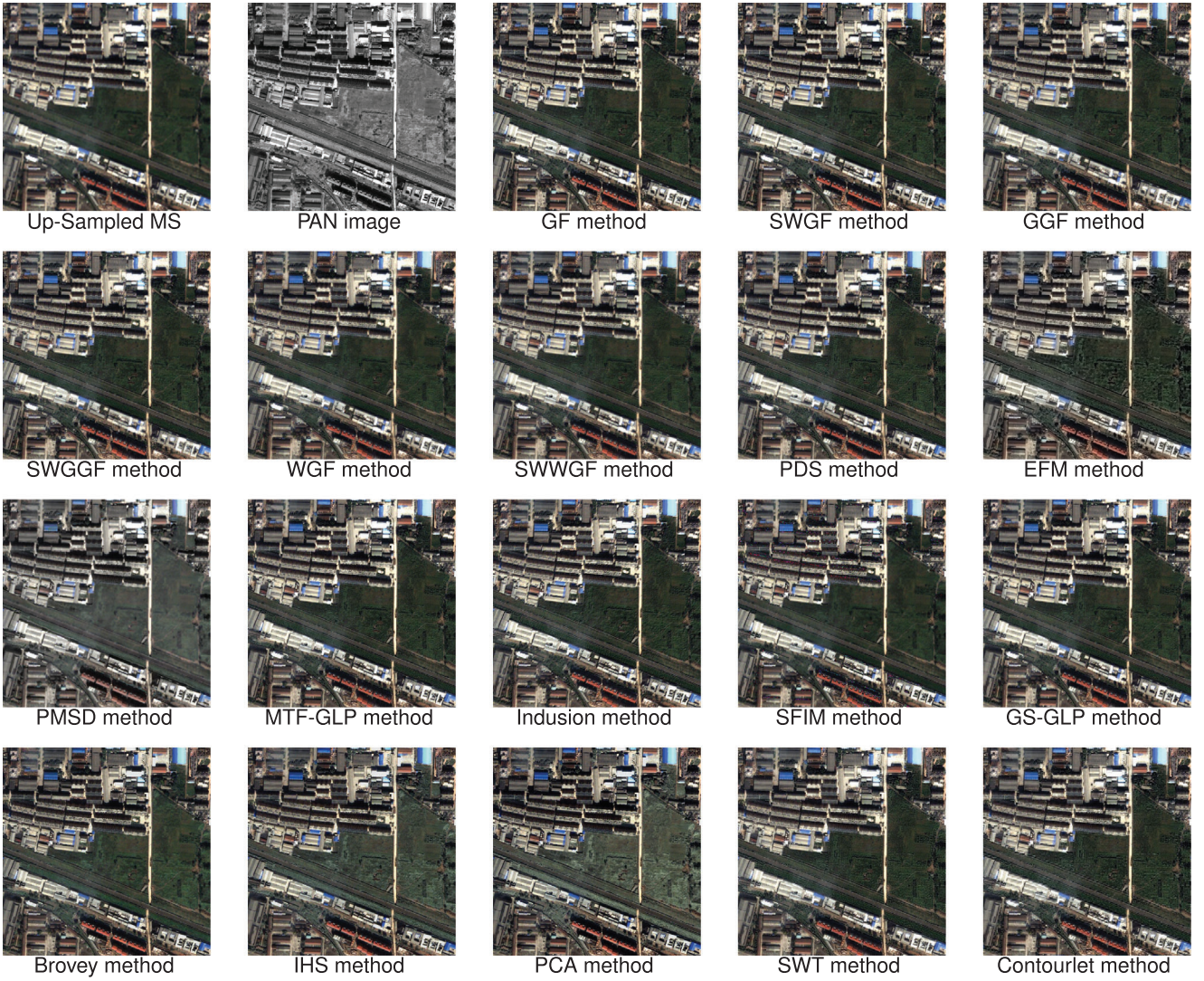
FIGURE 9 Fusion result of QuickBird real dataset

gradient guided filter GGF to obtain detailed information from high-frequency PAN image by estimating the difference between high-frequency PAN and its filtered version in which I component is used as a guidance image. The side window filtering was employed along with these filters. These filters can be used to minimise the difference between the I component and the low-pass filtered PAN image. Firstly, the difference between the filtered image Z_1 and the input image PAN_H is the detailed image D_1; secondly, the difference between the output filtering Z_1 and the output filtering Z_2 is the detailed image D_2, the final detailed information image D is estimated by the summation of D_1 and D_2. Note that, two stages of the filter are employed in order to acquire more details from the input image.

$$Z_1 = F\left(\text{PAN}_H, I, r, \xi\right), D_1 = \text{PAN}_H - Z_1 \quad (11)$$

where F represents the kernel filter type.

$$Z_2 = F\left(Z_1, I, r, \xi\right), D_2 = Z_1 - Z_2 \quad (12)$$

$$D = D_1 + D_2 \quad (13)$$

3.4 | Generating the fusion image

In this section, before generating the fusion image, the injection gain for each MS band is computed, which is defined by the quantity of the panchromatic image spatial detail information [35], which is being injected into the MS image.

$$g_{i'\text{th}} = \frac{\text{MS}_{i'\text{th}}}{1/N \sum_1^N \text{MS}_{i'\text{th}}} \left((1 - \beta_{i'\text{th}})w_{\text{PAN}} + \beta_{i'\text{th}}w_{\text{MS}_{i'\text{th}}}\right) \quad (14)$$
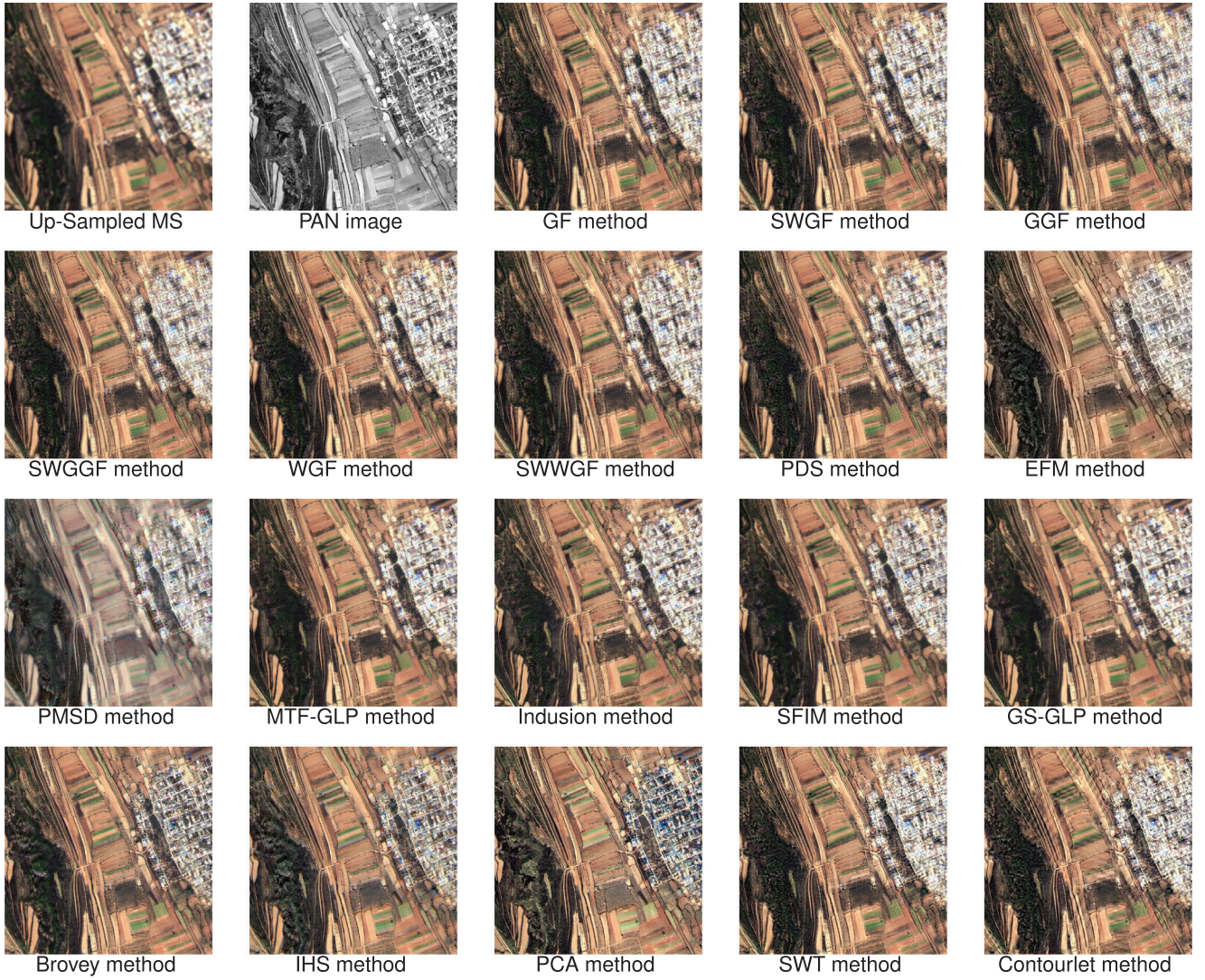
FIGURE 10 Fusion result of Gaofen real dataset

where $g_{i'\text{th}}$, $\beta_{i'\text{th}}$, and $w_{\text{MS}_{i'\text{th}}}$ indicate injection gain, trade-off parameter, and the edge detecting weighting matrix for i'th band, respectively. The edge detecting weighting matrix can be computed as follows:

$$w_{\text{img}} = \exp\left(-\frac{\lambda}{|\nabla\text{img}|^4 + \varepsilon}\right) \quad (15)$$

where $|\nabla\text{img}|$ represents a gradient of an image, λ, ε are the tuning parameters. Then, the fusion image can be estimated by the following equation

$$\text{HRMS} = \text{MS}_{i'\text{th}} + (D \times g_{i'\text{th}}) \quad (16)$$

4 | EXPERIMENTAL RESULTS

In order to provide solid results and to evaluate the proposed technique, different types of remote sensing datasets were evaluated. In total, five datasets have been selected for implementation purposes, three degraded datasets, and two real datasets. These datasets were acquired from different sensors. Namely, Ikonos, Quick-Bird, GeoEye for degraded datasets, and Gaofen, Quick-Bird for real datasets. However, the proposed model is compared with some existing fusion models whose codes are publicly available [5] such as PCA [11], IHS [10], Brovey [36], SFIM [37], GS-GLP [38, 39], Indusion [40], and MTF-GLP [41]. Furthermore, it is compared with SWT [42], Contourlet [19], and three state-of-the-art methods, includes PDS [20], EFM [21], and PMSD [6].

4.1 | Analysis of parameters setting

Before the implementation step, the parameters setting is analysed, the half-size of the Gaussian bilateral filter window w is set to 5, $G\sigma s$, $G\sigma r$ are 10, 0.3, respectively. Other filters used were based on two critical parameters, r, and ξ. Figure 2 illustrates the detailed examination of parameter sets. The first column in Figure 2 shows the performance of four quality indexes related to ξ including CC, IndexQ, UIQI, and SSIM. Considering that, the highest value means better performance. However, it can be seen that the performances of CC, IndexQ, and UIQI have all slightly increased associated with the increased value of r and ξ. The changing trend of the SSIM index has remained fairly stable in the first column of Figure 2 but in the last sub-Figure 2 of the first column at the bottom, there is a slight rise. The changing trends of ERG and SAM indexes are shown in the second column in Figure 2. Noticeably, there is a slight fluctuation but the smallest value for both indexes has illustrated when r is 8 and ξ is 0.4^2. The third column in Figure 2 illustrates the performance of PSNR, the changing trend has climbed in Figure 2, whereas it has remained stable when r is 4, and ξ is 0.2^2. Clearly, the best performance of the PSNR index is shown in Figure 2 when r is 8 and ξ is 0.4^2.

4.2 | Experiments on degraded data

Regarding the degraded datasets, the Ikonos satellite provides a four-band multispectral image with size 512×512 and a PAN image with 2048×2048. According to Wald's protocol [43], we degraded the original multispectral image by a factor of 4 using MTF filtering and decimation. The Quick-Bird and Geo-Eye satellites provide four multispectral image bands with size 64×64 and a PAN image with size 256×256. The fusion results of degraded datasets are shown in Figures 3, 5, and 7. We evaluate the fusion results based on eight quality metrics [5, 44]. Correlation coefficients CC, image quality indexes UIQI, Index Q, PSNR, and structural similarity index SSIM measures the similarity and the relevant information between a reference image and a fusion image. The highest value means better performance. Besides, the root means square error RMSE, error relative global adimensionnelle ERGAS, and the spectral angle mapper SAM, the lower value indicates better understanding.

From Figure 3, we can observe that the PMSD method produced unnatural colours in the obtained fused image and there are distortions in the spatial resolution. The fusion results of PCA, IHS, and Brovey methods produced better spatial enhancement results but still suffer from spatial distortions. The Indusion, SFIM, GS-GLP methods can perform better as compared to the spectral enhancement than the traditional methods, but the fused images have remarkable spatial distortions. There are some blurring areas in the fusion result of the SWGGF method. Although the PDS, EFM, SWT, and Contourlet methods preferably preserved details such as the edges, however, the colour information changed slightly. The effects of the proposed approach have large advantages at retaining the detailed information, and the detail contrast enhancement effect is high.

TABLE 4 Numerical evaluation for QickBird real dataset

Method	QNR (1)	D_s	D_λ
GF	0.9472	0.1124	0.078
SWGF	0.9476	0.1134	0.0783
WGF	0.9548	0.1010	0.0649
SWWGF	0.9552	0.0868	0.0733
GGF	**0.9717**	0.0639	**0.0410**
SWGGF	0.9585	0.0869	0.0621
PDS	0.9460	0.1146	0.0811
EFM	0.8816	0.2545	0.1653
PMSD	0.9215	0.1629	0.1179
MTF-GLP	0.93708	0.13929	0.09278
Indusion	0.96348	**0.03066**	0.08704
SFIM	0.93699	0.06634	0.14364
Brovey	0.9512	0.17315	0.05659
IHS	0.91008	0.2534	0.10823
PCA	0.90127	0.28645	0.13137
GS-GLP	0.94533	0.12337	0.07886
SWT	0.9314	0.1516	0.0974
Contourlet	0.9290	0.1499	0.1057

The numerical evaluation of fusion QuickBird degraded data is reported in Table 1. From the table, we can see that the SWGF method can provide the best values in most indexes. The fusion results of the Ikonos satellite dataset are shown in Figure 5. Considering both the spatial and spectral details, it can be observed that the proposed technique using WGF filter performed better than the comparative approaches, particularly spatial fidelity. Figure 7 shows the fusion results of the degraded GeoEye satellite dataset. It can be seen that the fusion results of PMSD, Brovey, IHS, PCA achieved severe spectral distortion. The other methods performed well, but there are some blurred areas at some places. Besides, the spatial and spectral distortions are obvious in the fusion result of SWWGF for Ikonos and GeoEye datasets. The numerical evaluation of fusion results for Figures 5 and 7 are given in Tables 2 and 3, respectively. It shows that the WGF method provides the best values in most evaluation indexes.

4.3 | Experiments on real data

In terms of real data (No reference image), two kinds were selected, QuickBird and Gaofen. The size of the MS image and PAN image is 256×265, 1024×1024, respectively. The fusion results of real datasets are shown in Figures 9 and 10. The real data is evaluated based on the QNR index, which depends on a spatial distortion index D_s and a spectral distortion index D_λ. Overall, by the subjective comparison of fusion results in Figures 9 and 10, the Brovey, IHS, PCA, and PMSD techniques suffered from spectral distortion. The other methods performed well but have insufficient ability to extract the detailed

TABLE 5 Numerical evaluation for Gaofen real dataset

Method	QNR (1)	D_s	D_λ
GF	0.8720	0.3272	0.1278
SWGF	0.8716	0.3378	0.1283
WGF	0.8757	0.3269	0.1265
SWWGF	0.8738	0.3294	0.1308
GGF	**0.8803**	0.3027	0.0877
SWGGF	0.8782	0.3446	0.1041
PDS	0.8794	0.3440	0.1388
EFM	0.8512	0.3938	0.2898
PMSD	0.8566	0.3685	0.1472
MTF-GLP	0.52872	0.36999	0.16077
Indusion	0.67597	**0.19653**	0.15868
SFIM	0.62588	0.29534	0.1118
Brovey	0.2967	0.64891	0.15492
IHS	0.24905	0.68984	0.19702
PCA	0.36387	0.64878	0.14299
GS-GLP	0.70576	0.2519	**0.05658**
SWT	0.8289	0.4154	0.1924
Contourlet	0.8173	0.4302	0.2168

TABLE 6 Time comparison (in second)

Method	Time
PCA	0.06
IHS	0.01
Brovey	0.01
SFIM	0.04
Indusion	0.07
MTF-GLP	0.22
GS-GLP	0.19
SWT	0.78
Contourlet	0.40
PDS	7.52
EFM	0.07
PMSD	0.31
GF	1.88
SWGF	4.51
GGF	1.59
SWGGF	4.99
WGF	1.69
SWWGF	4.47

information. Therefore, the objective numerical evaluation of Figures 9 and 10 are given in Tables 4 and 5, respectively.

Table 4 shows that the GGF method can provide the best values in terms of QNR, D_λ metrics. The Indusion method has the best value in terms of spatial fidelity, followed by the GGF method. Table 5 illustrates that the GGF method can provide the best values in the QNR metric. The GS-GLP method has the best value in terms of spectral fidelity, followed by the GGF method.

5 | DISCUSSION

In this study, we proposed a pansharpening method that uses different kinds of filters for image fusion. The performance of pansharpening methods was evaluated using various standard quality measures. The remarkable exhibitions of those filters can be plausibly explained by the way that the techniques used depend on the same criteria and utilise comparative instruments to accomplish the objective of pansharpening.

The size of filter window r, which determines the huge distinction of the guided image in neighbourhood windows, and normalised parameter ξ, which determines the haze level of the filter are set as 8, 0.4^2, respectively. Given the estimations of assessment indexes, which are discussed previously. In this manner, we exploit the PAN image to accomplish the spatial upgradation. Our goal is to limit the spectral distortion by infusing a point-by-point vector corresponding to the resampled MS vector. In this way, colours are preserved in terms

of hue, while saturation might be changed. In this study, three degraded datasets were implemented. The spatial subtleties in the combination images of all techniques were upgraded, yet some spatial data were improved unduly. In visual comparison, it was observed that most pansharpening techniques performed well in terms of spatial fidelity. The PDS, EFM, and PMSD methods show some colour changes compared with a reference image, especially the PMSD method because these methods are more focused on spatial details than spectral details. Due to the difficulties of visual evaluation for humans, we estimated error maps (A difference between fused image and reference image), as illustrated in Figures 4, 6, and 8. The results were evaluated based on some quality metrics. The SWGF method performs a significant objective effect in ERGAS, SAM, RMSE, UIQI, and PSNR. Thereby, SWGF still ranks in the top range for QuickBird data and balances spectral and spatial fidelity.

Overall, for Ikonos and GeoEye degraded datasets, the WGF performs a significant objective effect among the quality metrics. Despite this, applying the side window kernel with the weighted guided filter SWWGF does not perform well as compared to other filters regrading. The Experiments were also conducted on two groups of real datasets. The QNR and D_λ values of the GGF method are better than those of the other methods, indicating that the GGF method produces a higher quality fusion result. Furthermore, in terms of D_λ index for real Gaofen data, the GS-GLP method performed the best value, followed by the GGF. Thus, the GGF method performed better concerning real datasets as compared to other techniques.

6 | CONCLUSIONS

This study proposed an image fusion technique based on different kinds of guided filter to acquire the high-resolution multi-spectral image. The study aimed at enhancing the spatial resolution of the MS image corresponding to the PAN image while preserving the spectral resolution. The elaborated simulations for different kinds of images and the experimental comparison results indicated that the proposed model had performed efficiently for image fusion tasks supported with higher computational efficiencies. The technique was tested on several remote sensing datasets, and the experimental evaluation results indicated different filters' decent performance for different datasets used in this study.

To sum up, the proposed method performs well as compared to other techniques. We have indicated that the side window local linear filters may have the potential to be used excellently for image fusion.

ORCID

Ahmad AL Smadi https://orcid.org/0000-0003-3487-8041

REFERENCES

1. Lakhal, M.I., et al.: Recurrent neural networks for remote sensing image classification. IET Comput. Vision 12(7), 1040–1045 (2018)
2. Reddy, G.O.: Satellite remote sensing sensors: Principles and applications. In: Geospatial Technologies in Land Resources Mapping, Monitoring and Management, pp. 21–43.Springer, Berlin, Heidelberg (2018)
3. Ma, J., et al.: Fusiongan: A generative adversarial network for infrared and visible image fusion. Information Fusion 48, 11–26 (2019)
4. Ma, J., et al.: Pan-GAN: An unsupervised learning method for pan-sharpening in remote sensing image fusion using a generative adversarial network. Information Fusion 62, 110–120 (2020)
5. Vivone, G., et al.: A critical comparison among pansharpening algorithms. IEEE Trans. Geosci. Remote Sens. 53(5), 2565–2586 (2014)
6. Al.Smadi, A., Abugabah, A.: Intelligent information systems and image processing: A novel pan-sharpening technique based on multiscale decomposition. In: Proceedings of the 2018 the 2nd International Conference on Video and Image Processing, pp. 208–212.ACM Press, New York (2018)
7. Alsmadi, A., Yang, S., Zhang, K.: Pansharpening via deep guided filtering network. International Journal of Image Processing and Visual Communication 5, 1–8 (2018)
8. Dou, W., et al.: A general framework for component substitution image fusion: An implementation using the fast image fusion method. Computers Geosciences 33(2), 219–228 (2007)
9. Park, J.H., Kim, K.O., Yang, Y.K.: Image fusion using multiresolution analysis. In: IGARSS 2001. Scanning the Present and Resolving the Future. Proceedings. IEEE 2001 International Geoscience and Remote Sensing Symposium, pp. 864–866.IEEE, Piscataway, NJ (2001)
10. Carper, W., Lillesand, T., Kiefer, R.: The use of intensity-hue-saturation transformations for merging spot panchromatic and multispectral image data. Photogramm. Eng. Remote Sens. 56(4), 459–467 (1990)
11. Kwarteng, P., Chavez, A.: Extracting spectral contrast in landsat thematic mapper image data using selective principal component analysis. Photogramm. Eng. Remote Sens. 55, 339–348 (1989)
12. Laben, C.A., Brower, B.V.: Process for enhancing the spatial resolution of multispectral imagery using pan-sharpening. US Patent 6,011,875, 4 Jan 2000
13. Kang, X., Li, S., Benediktsson, J.A.: Pansharpening with matting model. IEEE Trans. Geosci. Remote Sens. 52(8), 5088–5099 (2013)
14. Xu, Q., et al.: High-fidelity component substitution pansharpening by the fitting of substitution data. IEEE Trans. Geosci. Remote Sens. 52(11), 7380–7392 (2014)
15. Amro, I., et al.: A survey of classical methods and new trends in pansharpening of multispectral images. EURASIP Journal on Advances in Signal Processing 2011(1), 1–22 (2011)
16. Burt, P.J., Adelson, E.H.: The laplacian pyramid as a compact image code. In: Readings in Computer Vision, pp. 671–679.Elsevier, New York (1987)
17. Mallat, S.G.: A theory for multiresolution signal decomposition: the wavelet representation. IEEE Trans. Pattern Anal. Mach. Intell. 11(7), 674–693 (1989)
18. Nason, G.P., Silverman, B.W.: The stationary wavelet transform and some statistical applications. In: Wavelets and statistics, pp. 281–299.Springer, Berlin, Heidelberg (1995)
19. Do, M.N., Vetterli, M.: The contourlet transform: an efficient directional multiresolution image representation. IEEE Trans. Image Process. 14(12), 2091–2106 (2005)
20. Jian, L., et al.: Pansharpening using a guided image filter based on dual-scale detail extraction. J. Ambient Intell. Hum. Comput. 9, 1–15 (2018)
21. Li, X., Qi, W., Yue, S.: An effective pansharpening method based on guided filtering. In: 2016 IEEE 11th Conference on Industrial Electronics and Applications, pp. 534–538.IEEE, Piscataway, NJ (2016)
22. Pal, C., Chakrabarti, A., Ghosh, R.: A brief survey of recent edge-preserving smoothing algorithms on digital images. arXiv:150307297, (2015)
23. Farbman, Z., et al.: Edge-preserving decompositions for multi-scale tone and detail manipulation. ACM Trans. Graphics 27(3), 1–10 (2008)
24. Rudin, L.I., Osher, S., Fatemi, E.: Nonlinear total variation based noise removal algorithms. Physica D: Nonlinear Phenomena 60(1–4), 259–268 (1992)
25. Paris, S.: A gentle introduction to bilateral filtering and its applications. In: ACM SIGGRAPH 2007 courses, pp. 1–50.ACM Press, New York (2007)
26. He, K., Sun, J., Tang, X.: Guided image filtering. IEEE Trans. Pattern Anal. Mach. Intell. 35(6), 1397–1409 (2012)
27. Yin, H., Gong, Y., Qiu, G.: Side window guided filtering. Signal Processing 165, 315–330 (2019)
28. Tomasi, C., Manduchi, R.: Bilateral filtering for gray and color images. In: Sixth International Conference on Computer Vision, pp. 839–846.IEEE, Piscataway, NJ (1998)
29. Hu, J., Li, S.: The multiscale directional bilateral filter and its application to multisensor image fusion. Information Fusion 13(3), 196–206 (2012)
30. Qiu, X., et al.: Guided filter-based multi-focus image fusion through focus region detection. Signal Process. Image Commun. 72, 35–46 (2019)
31. Li, Z., et al.: Weighted guided image filtering. IEEE Trans. Image Process. 24(1), 120–129 (2014)
32. Kou, F., et al.: Gradient domain guided image filtering. IEEE Trans. Image Process. 24(11), 4528–4539 (2015)
33. Yin, H., Gong, Y., Qiu, G.: Side window filtering. In: Proceedings of the IEEE Conference on Computer Vision and Pattern Recognition, pp. 8758–8766.IEEE, Piscataway, NJ (2019)
34. Rahmani, S., et al.: An adaptive ihs pan-sharpening method. IEEE Geosci. Remote Sens. Lett. 7(4), 746–750 (2010)

35. Yang, Y., et al.: Remote sensing image fusion based on adaptive ihs and multiscale guided filter. IEEE Access 4, 4573–4582 (2016)

36. Gillespie, A.R., Kahle, A.B., Walker, R.E.: Color enhancement of highly correlated images. ii. channel ratio and chromaticity transformation techniques. Remote Sens. Environ. 22(3), 343–365 (1987)

37. Liu, J.: Smoothing filter-based intensity modulation: A spectral preserve image fusion technique for improving spatial details. Int. J. Remote Sens. 21(18), 3461–3472 (2000)

38. Aiazzi, B., et al.: Mtf-tailored multiscale fusion of high-resolution ms and pan imagery. Photogrammetric Engineering & Remote Sensing 72(5), 591–596 (2006)

39. Alparone, L., et al.: Comparison of pansharpening algorithms: Outcome of the 2006 GRS-S data-fusion contest. IEEE Trans. Geosci. Remote Sens. 45(10), 3012–3021 (2007)

40. Khan, M.M., et al.: Indusion: Fusion of multispectral and panchromatic images using the induction scaling technique. IEEE Geosci. Remote Sens. Lett. 5(1), 98–102 (2008)

41. Aiazzi, B., et al.: Context-driven fusion of high spatial and spectral resolution images based on oversampled multiresolution analysis. IEEE Trans. Geosci. Remote Sens. 40(10), 2300–2312 (2002)

42. Li, S., Kwok, J.T., Wang, Y.: Using the discrete wavelet frame transform to merge landsat TM and spot panchromatic images. Information Fusion 3(1), 17–23 (2002)

43. Wald, L.: Data Fusion: Definitions and Srchitectures: Fusion of Images of Different Spatial Resolutions, Presses des MINES, Paris (2002)

44. Jagalingam, P., Hegde, A.V.: A review of quality metrics for fused image. Aquat. Procedia 4, 133–142 (2015)